Multimode parity-time symmetry and loss compensation in coupled waveguides with loss and gain

Anton V. Hlushchenko
State Key Laboratory of Integrated Optoelectronics, College of Electronic Science and Engineering, International Center of Future Science, Jilin University, 2699 Qianjin Street, Changchun 130012, China
and National Science Center "Kharkiv Institute of Physics and Technology" of National Academy of Sciences of Ukraine, 1, Akademicheskaya Street, Kharkiv 61108, Ukraine

Vitalii I. Shcherbinin
National Science Center "Kharkiv Institute of Physics and Technology" of National Academy of Sciences of Ukraine, 1, Akademicheskaya Street, Kharkiv 61108, Ukraine

Denis V. Novitsky
B. I. Stepanov Institute of Physics, National Academy of Sciences of Belarus, 68 Nezavisimosti Avenue, Minsk 220072, Belarus

Vladimir R. Tuz*
State Key Laboratory of Integrated Optoelectronics, College of Electronic Science and Engineering, International Center of Future Science, Jilin University, 2699 Qianjin Street, Changchun 130012, China

(Received 23 April 2021; accepted 21 June 2021; published 6 July 2021)

Loss compensation via inserting gain is of fundamental importance in different branches of photonics, nanoplasmonics, and metamaterial science. This effect has found an impressive implementation in the parity-time symmetric ($\mathcal{PT}$-symmetric) structures possessing balanced distribution of loss and gain. In this paper, we generalize this phenomenon to the asymmetric systems demonstrating loss compensation in the coupled multimode loss-gain dielectric waveguides of different radii. We show that similar to the $\mathcal{PT}$-symmetric coupled single-mode waveguides of identical radii, the asymmetric systems support the exceptional points called here the loss-compensation (LC) thresholds where the frequency spectrum undergoes a transition from complex to real values. Moreover, the LC thresholds can be obtained for dissimilar modes excited in the waveguides providing an additional degree of freedom to control the system response. In particular, changing loss and gain of asymmetric coupled waveguides, we observe loss compensation for TM and TE modes as well as for the hybrid HE and EH modes.

DOI: 10.1103/PhysRevA.104.013507

I. INTRODUCTION

The intriguing properties of loss-gain distributions are the subject of the fast-growing field of non-Hermitian photonics. The most notable and studied class of non-Hermitian systems is the $\mathcal{PT}$-symmetric systems which possess the perfectly balanced spatial distribution of gain and loss [1–3]. $\mathcal{PT}$ symmetry guarantees the reality of non-Hermitian Hamiltonian spectra [4] that have been readily implemented and observed in the optical domain [5,6]. Subsequently, $\mathcal{PT}$ symmetry was transferred to electronic circuits [7], acoustics [8], and time-varying (Floquet) systems [9].

The balance between loss and gain helps to solve the problem of loss compensation which is of paramount importance for the efficiency of plasmonic and metamaterial-based devices [10–12]. The loss-compensation effect proved to be connected to another remarkable feature of non-Hermitian systems—the possibility of specific degeneracies called exceptional points (EPs) which were observed in photonics [13,14] as well as in acoustics [15]. In contrast to the degeneracies of Hermitian systems (the so-called diabolic points) with coalescing eigenvalues, the EPs imply coalescence of both eigenvalues and eigenfunctions. In the $\mathcal{PT}$-symmetric systems, the EPs mark the points of phase transitions between the $\mathcal{PT}$-symmetric phase and the phase with spontaneously broken $\mathcal{PT}$ symmetry. It is important to emphasize, however, that the EPs are the general phenomenon observed also in purely passive systems (such as whispering-gallery-mode microresonators [16], ring cavities [17], anisotropic waveguides [18]), and even in the systems with radiative loss only [19].

The EPs have become a workhorse of many recent achievements, such as enhanced perturbation sensing [20,21], novel lasing schemes [22,23], the enhanced Sagnac effect for laser gyroscopes [24,25], simultaneous coherent perfect absorption and amplification [26,27], asymmetric transmission [5,28], etc. An interesting feature of EPs is their topological nature which can be revealed with their dynamical encircling in parameter space and can be used for mode switching [29], mode transfer [30], and polarization conversion [31]. Another

*tvr@jlu.edu.cn

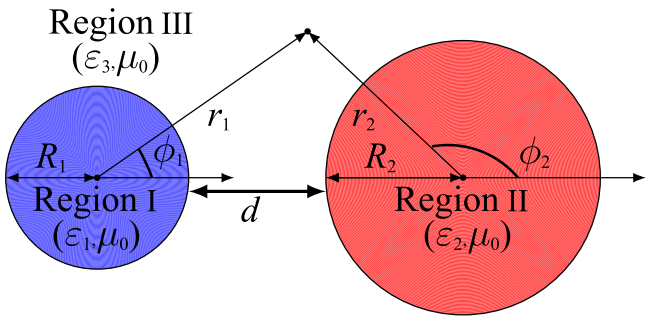

FIG. 1. Geometry of unequally sized dielectric waveguides immersed in an infinite medium.

exciting direction is the observation and utilization of the higher-order EPs where more than two eigenmodes coalesce. Such EPs can be realized either in the systems containing three or more resonant elements [21,32,33] or by hybridizing several usual (second-order) EPs [34–36]. It should be noted that the most considerations of non-Hermitian effects are limited to the single-mode case with the use of the coupled-mode theory [37]. The multimode platforms provide much richer opportunities in controlling optical response and dynamics as evidenced by the examples of dispersion engineering and mode conversion in the waveguide and microresonator systems [38–40].

For the symmetric system of coupled dielectric waveguides, the full loss compensation is possible only for the perfect balance between gain and loss corresponding to the nonviolated $\mathcal{PT}$ symmetry [6]. This poses rather tough and difficult-to-achieve conditions for experimental realization of the related effects [13]. On the contrary, for the asymmetric system, the full loss compensation can be reached even for the unbalanced gain and loss. By analogy with the $\mathcal{PT}$ symmetry, this generalized situation can be called the loss-compensation (LC) symmetry [41,42]. In this paper, we propose further generalization demonstrating LC phenomenon for the coupled dissimilar waveguides under excitation of the modes with the same or different azimuthal indices. In dielectric waveguides, all modes except TE and TM are hybrid, i.e., they have axial components of both electric and magnetic fields. Therefore, to analyze the system, we apply the multimode approach [42,43] which allows us to obtain exact solutions of the eigenvalue problem for all possible classes of modes supported by the asymmetric guiding structure. We show that such an asymmetric structure supports specific EPs called the LC thresholds and reached for different loss-gain ratios depending on the modes used. Thus, the mode composition of the non-Hermitian system is an additional degree of freedom useful for tuning the parameters necessary to obtain the constant-intensity modes [44,45] and other applications.

II. MULTIMODE ANALYTICAL APPROACH

For our analysis, we use the multimode analytical approach [43], which was previously successfully applied to coupled systems with loss and gain [42]. Following Ref. [42], we consider a pair of coupled dielectric cylinders of the radii R_1 and R_2 placed in an ambient medium. Figure 1 shows the cross sections of the dielectric circular waveguides with the permittivities ε_1 and ε_2, respectively (Regions I and II). The polar coordinate systems associated with the waveguides are denoted as (r_1, ϕ_1) and (r_2, ϕ_2). The waveguides are placed in the infinite uniform medium (Region III) with the real-valued permittivity ε_3. The permeability $\mu = \mu_0$ is assumed to be the same in all regions. Without loss of generality, we suppose that the first waveguide contains lossy medium and the second one contains gain material [$\mathrm{Im}(\varepsilon_1) < 0$ and $\mathrm{Im}(\varepsilon_2) > 0$], whereas $\mathrm{Re}(\varepsilon_1) > \varepsilon_3$ and $\mathrm{Re}(\varepsilon_2) > \varepsilon_3$.

In order to solve the eigenvalue problem for this system, we write the electromagnetic fields in every region using the corresponding polar coordinates as shown in Fig. 1. For example, the E_z and H_z components of electromagnetic fields in Region I are written in terms of the local coordinates (r_1, ϕ_1) as

$$E_z^1 = \sum_{n=-N}^{N} A_n^1 J_n(k_{p,1} r_1) e^{in\phi_1},$$
$$H_z^1 = \sum_{n=-N}^{N} B_n^1 J_n(k_{p,1} r_1) e^{in\phi_1}, \tag{1}$$

whereas in Region II the local coordinates (r_2, ϕ_2) are used as

$$E_z^2 = \sum_{n=-N}^{N} A_n^2 J_n(k_{p,2} r_2) e^{in\phi_2},$$
$$H_z^2 = \sum_{n=-N}^{N} B_n^2 J_n(k_{p,2} r_2) e^{in\phi_2}, \tag{2}$$

and, finally, in Region III we have the contributions from both local coordinate systems,

$$E_z^3 = \sum_{n=-N}^{N} C_n^1 H_n^{(1,2)}(k_{p,3} r_1) e^{in\phi_1} + \sum_{n=-N}^{N} C_n^2 H_n^{(1,2)}(k_{p,3} r_2) e^{in\phi_2},$$
$$H_z^3 = \sum_{n=-N}^{N} D_n^1 H_n^{(1,2)}(k_{p,3} r_1) e^{in\phi_1} + \sum_{n=-N}^{N} D_n^2 H_n^{(1,2)}(k_{p,3} r_2) e^{in\phi_2}. \tag{3}$$

Here $\{A_n^1, A_n^2, B_n^1, B_n^2, C_n^1, C_n^2, D_n^1, D_n^2\}$ are the unknown amplitudes of azimuthal harmonics, $k_{p,j}^2 = k_j^2 - k_z^2$, $k_j = k_0 \varepsilon_{r_j}$ $(j = 1\text{–}3)$, $\varepsilon_{r_j} = \varepsilon_j/\varepsilon_0$ is the relative permittivity, $k_0^2 = \omega^2 \varepsilon_0 \mu_0$, J_n is the Bessel function, $H_n^{(1)}$ and $H_n^{(2)}$ are the Hankel functions of the first and second kinds, respectively, and the field factor of the form $\exp[-i(\omega t - k_z z)]$ is assumed and omitted. The choice of the Hankel function is governed by the boundary conditions for the fields in Region III as follows: $E_z^3 \to 0$ and $H_z^3 \to 0$ for $r_1, r_2 \to \infty$.

Since the derivation of other field components is cumbersome, it is relegated to the Appendix. We only note that the Maxwell equations and Eqs. (1)–(3) allow us to obtain the expressions for the electromagnetic-field

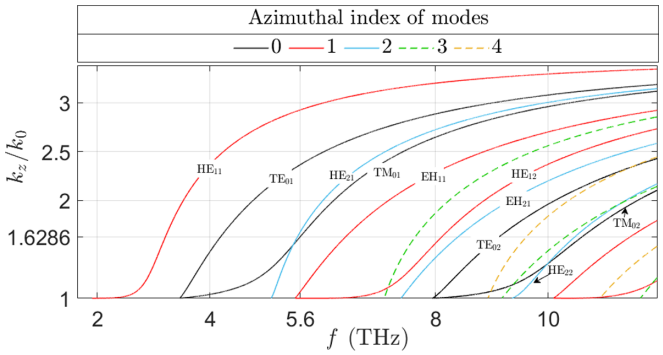

FIG. 2. Lowest-order modes of the circular dielectric waveguide with $\epsilon_r = 12$ and $R = 10$ μm.

components E_ϕ and H_ϕ in every region. The unknown coefficients $\{A_n^1, A_n^2, B_n^1, B_n^2, C_n^1, C_n^2, D_n^1, D_n^2\}$ and k_z can be obtained from the dispersion relation derived using the continuity conditions for the tangential fields at the boundary surfaces $r_1 = R_1$ and $r_2 = R_2$ (see the Appendix).

Thus, in the general case, the solution of the boundary-value problem for a pair of dielectric cylinders has a form of coupled azimuthal harmonics, which include propagating and evanescent modes. These modes supported by the first (second) cylinder can be classified as TM_{0m} and TE_{0m} modes with nonzero amplitudes A_0^1 (A_0^2) and B_0^1 (B_0^2) of the core field, respectively, and hybrid HE_{nm} and EH_{nm} modes with amplitudes A_n^1 and B_n^1 (A_n^2 and B_n^2) [46]. As the distance d between cylinders approaches infinity, the coupling between harmonics vanishes, and the modes of uncoupled dielectric cylinders transform to pure TE, TM, or hybrid modes (Fig. 2). In the following, the modes of a pair of dielectric cylinders are designated as TM_{0m}, TE_{0m}, HE_{nm}, and EH_{nm} modes, depending on their behavior in the extreme case $d \to \infty$. In the operating mode pair, the first and the second modes are related to the first (lossy) and the second (gainy) cylindrical waveguides, respectively.

III. TM AND TE MODES

A. Single waveguide modes

Our aim is to demonstrate the possibility of full loss compensation for the coupled dielectric waveguides with gain and loss supporting different modes with an arbitrary value of the azimuthal index. The dispersion relations of coupled waveguides will tend to the dispersion relations of independent waveguides with increasing distance between them. Therefore, we are interested in the crossing points of the dispersion curves of two independent cylinders. The dispersion curves for the lowest-order modes of a single waveguide are shown in Fig. 2. Changing the radius or permittivity of another cylinder, one can observe the shift of its dispersion curves with respect to the curves of the first one. Thus, for any pair of modes, we can find their crossing points at a required frequency f and longitudinal wave number k_z/k_0. We will show further that these crossing points are convenient for the realization of full loss compensation at the certain values of gain-loss parameter and distance between the cylinders.

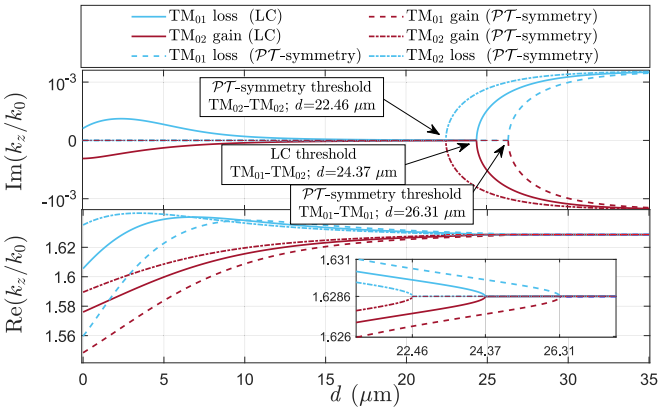

FIG. 3. The real and imaginary parts of the eigenvalues k_z/k_0 for the TM modes as a function of the distance d between the coupled waveguides. LC and $\mathcal{PT}$-symmetry thresholds of TM-type modes are shown with arrows.

Let us consider, for the moment, the family of transverse electric TE_{0m} and transverse magnetic TM_{0m} modes of the circular cylindrical waveguide. As representatives of these modes, we choose the set $\{\mathrm{TM}_{01}, \mathrm{TM}_{02}, \mathrm{TE}_{01}, \mathrm{TE}_{02}\}$. For example, for the TM_{01} (TE_{01}) mode, we can choose an arbitrary solution of the dispersion relation (f; k_z/k_0). Then, we increase the cylinder radius to obtain same solution for the TM_{02} (TE_{02}) mode. The initial and increased radii of the waveguide can serve as a first approximation to find the conditions of loss compensation for the coupled cylinders with gain and loss. For instance, according to Fig. 2, the values of $f = 5.6$ THz and $k_z/k_0 = 1.6286$ correspond to the TM_{01} (TE_{01}) mode of the waveguide with $\epsilon_{r1} = 12$ and $R_1 = 10$ μm and to the TM_{02} (TE_{01}) mode of the waveguide with $\epsilon_{r2} = 12$ and $R_2 = 18.93$ μm ($R_2 = 16.305$ μm).

B. Symmetric coupled waveguides: $\mathcal{PT}$ symmetry

We start with the case of symmetric system consisting of the coupled waveguides with the same radii and permittivities, i.e., $R_1 = R_2$ and $\epsilon_{r1} = \epsilon_{r2}$. In the case of balanced loss and gain, when the loss tangents have the same absolute value of $\tan\delta_1 = -\tan\delta_2$, this system is a $\mathcal{PT}$-symmetric one. $\mathcal{PT}$-symmetric systems can exist in two states: a $\mathcal{PT}$-symmetric state with the loss exactly compensated by gain and the broken-$\mathcal{PT}$-symmetry state with the violated compensation. In our case, the transition between these states can be realized by changing the distance between the cylinders. The point of transition where the $\mathcal{PT}$ symmetry gets broken is the EP where the modes of the system are degenerate. For example, in Fig. 3, the dashed and dashed-dot lines correspond to the TM_{01} and TM_{02} modes of the coupled waveguides with balanced gain and loss (the parameters are $R_1 = R_2 = 10$ μm, $\epsilon_{r1} = \epsilon_{r2} = 12$, $\tan\delta_1 = -\tan\delta_2 = 5\times10^{-4}$ for TM_{01} and $R_1 = R_2 = 18.93$ μm, $\epsilon_{r1} = \epsilon_{r2} = 12$, $\tan\delta_1 = -\tan\delta_2 = 4.05\times10^{-4}$ for TM_{02}), whereas in Fig. 4, the dashed and dashed-dot lines correspond to the TE_{01} and TE_{02} modes of the system with another set of parameters ($R_1 = R_2 = 7.48$ μm, $\epsilon_{r1} = \epsilon_{r2} = 12$, $\tan\delta_1 = -\tan\delta_2 = 5\times10^{-4}$ for TE_{01} and $R_1 = R_2 = 16.305$ μm, $\epsilon_{r1} = \epsilon_{r2} = 12$, $\tan\delta_1 = -\tan\delta_2 = 4.09\times10^{-4}$ for TE_{02}, respectively).

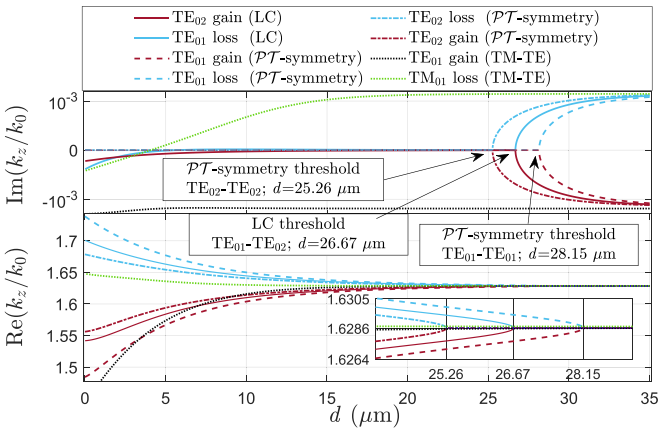

FIG. 4. The real and imaginary parts of the eigenvalues k_z/k_0 for the TE modes as a function of the distance d between the coupled waveguides. LC and $\mathcal{PT}$-symmetry thresholds of TE-type modes are shown with arrows.

The EPs are denoted as the $\mathcal{PT}$-symmetry thresholds since below these points (for distances shorter than the threshold one) the eigenvalues k_z/k_0 become purely real, and the system falls into the $\mathcal{PT}$-symmetric state. This state is preserved to the very connection of the cylinders at $d = 0$. It is important to note that due to the symmetry of the system, the full loss compensation via the $\mathcal{PT}$-symmetric state formation is observed only for the identical modes of both waveguides.

C. Asymmetric coupled waveguides: loss compensation

Although $\mathcal{PT}$-symmetric systems allow perfect loss compensation, it is often problematic to reach the ideal symmetry and the ideal loss-gain balance in realistic situations. Here, we show that loss compensation can be obtained in asymmetric systems with unequal coupled waveguides. Such a situation can be described as LC symmetry [41], which has much in common with $\mathcal{PT}$ symmetry (e.g., the existence of EPs), but at the same time, the requirements for system symmetry are strongly relaxed. Moreover, the LC phenomenon is reached for a pair of different modes as will be illustrated further.

Let us take the loss tangent of the first cylinder equal to $\tan\delta_1 = 5\times10^{-4}$ corresponding to the value for silicon [47]. Changing the gain tangent $\tan\delta_2$ and the distance between the cylinders d, we can obtain the full loss compensation at the target frequency $f = 5.6$ THz and wave-number $k_z/k_0 = 1.6286$. For the TE_{01} and TE_{02} modes, the EP which we call the LC threshold is reached at the system parameters as follows: $R_1 = 7.48$, $R_2 = 16.305$, $\epsilon_{r1} = \epsilon_{r2} = 12$, $d = 26.67\ \mu$m, $\tan\delta_2 = -4.05\times10^{-4}$ (see Fig. 5, dashed lines). For the modes TM_{01} and TM_{02}, the EP is reached at $d = 24.37\ \mu$m and $\tan\delta_2 = -4.05\times10^{-4}$ (see Fig. 5, solid lines). Similar to the $\mathcal{PT}$-symmetry threshold, the LC threshold corresponds to the purely real eigenvalues k_z/k_0. This approach can be utilized to obtain the EPs of full loss compensations for other pairs of modes as well. In Figs. 3 and 4, the LC thresholds are shown for the TM-type and TE-type modes, respectively, and compared to the $\mathcal{PT}$-symmetry thresholds. One can see that the LC thresholds for the different modes (for example, TM_{01} and TM_{02}) lie between the $\mathcal{PT}$-symmetry

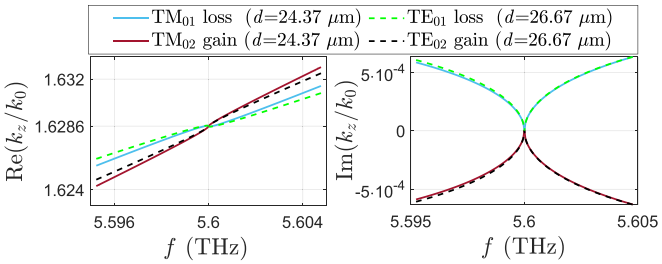

FIG. 5. EPs corresponding to the crossing of the pair of modes TM_{01}-TM_{02} and TE_{01}-TE_{02}.

thresholds for the corresponding individual modes. The main difference with the $\mathcal{PT}$-symmetric case is that the eigenvalues for the asymmetric waveguides do not remain real below the LC threshold. In fact, full loss compensation is realized only for a certain distance between dielectric cylinders. A further decrease in d gives rise to uncompensated losses in the system. In this process, the amplitudes of higher azimuthal harmonics increase [Fig. 6(a)]. This results in broken axial symmetry of the fields localized in the first (lossy) and the second (gainy) dielectric cylinders [Figs. 6(b)–6(d)] and is typical of both symmetric and asymmetric pairs of coupled waveguides.

The position of the LC threshold depends on the loss tangent and the frequency at which the dispersion curves cross. An example of electric- and magnetic-field distributions at the LC threshold and dots of broken symmetry for dissimilar waveguides are shown in Figs. 6(c) and 7(e) and 6(b) and 7(d) as compared to the distributions at the $\mathcal{PT}$-symmetry thresholds and the case of broken $\mathcal{PT}$ symmetry for the identical waveguides in Figs. 7(b) and 7(a). The smaller the loss tangent and the nearer the crossing to the cutoff frequency, the longer the distance between the waveguides corresponding to the threshold [42].

Thus, the LC threshold in the asymmetric system allows one to fully compensate the loss for the unbalanced gain and loss of the individual cylinders. This effect can be considered as a generalization of $\mathcal{PT}$-symmetric loss compensation since both the dispersion curves and the behavior of electromagnetic

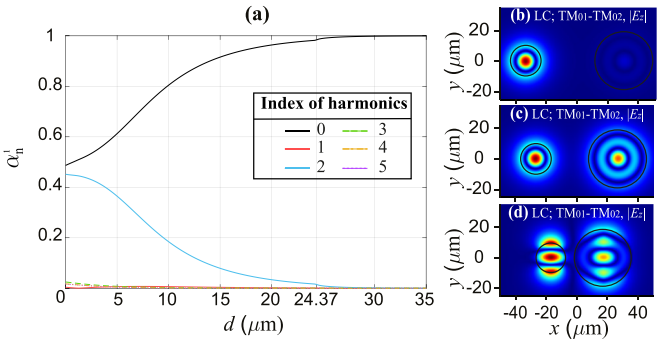

FIG. 6. (a) Normalized amplitudes $\alpha_n^1 = |A_n^1|/\sum_n |A_n^1|$ of azimuthal harmonics for lossy TM_{01} mode [see the solid blue (light gray) line in Fig. 3]. (b)–(d) Electric-field component $|E_z|$ of the lossy TM_{01} mode for the distances $d = 35$, $d = 24.37\ \mu$m (LC threshold) and $d = 5\ \mu$m between the asymmetric waveguides with the radii $R_1 = 10$ and $R_2 = 18.93\ \mu$m.

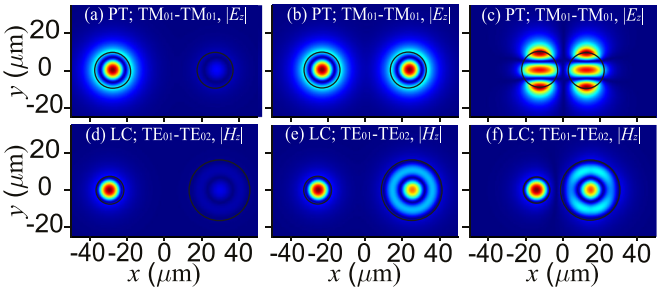

FIG. 7. (a)–(c) Axial electric-field $|E_z|$ of the lossy TM_{01} mode for the distances $d = 35$, $d = 26.31$ μm ($\mathcal{PT}$-symmetry threshold) and $d = 5$ μm between $\mathcal{PT}$-symmetric waveguides with the radii $R_1 = R_2 = 10$ μm. (d)–(f) Magnetic-field component $|H_z|$ of the lossy TE_{01} mode for the distances $d = 35$, $d = 26.67$ μm (LC threshold) and $d = 5$ μm between two asymmetric dielectric waveguides with the radii $R_1 = 7.48$, $R_2 = 16.305$ μm.

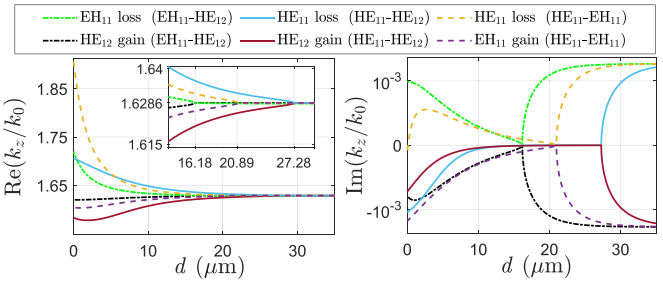

FIG. 8. Loss compensation for the hybrid modes with the azimuthal index 1.

fields show that the nature of loss-compensation phenomenon in asymmetric systems is similar to the $\mathcal{PT}$ symmetry in symmetric ones.

IV. HYBRID MODES: LOSS COMPENSATION

A. Modes with the same azimuthal index

We have shown above how the LC phenomenon and $\mathcal{PT}$ symmetries can be observed by coupling either TM or TE modes of the pair of cylindrical waveguides. However, when one mode is the TM one and another is the TE one, we cannot obtain an EP due to the weak coupling between the modes of different types (see Fig. 4, dotted line). In order to get around this problem, in this section, we consider the possibility of the LC phenomenon for the hybrid modes, which can be treated as a linear superposition of the corresponding TE and TM modes. These modes having both the electric- and magnetic-field components in the longitudinal direction can be either of HE type (magnetic component dominates) or EH type (electric component dominates).

We tune the dispersion curves for two cylinders to obtain the LC thresholds of hybrid modes for the same parameters ($f = 5.6$ THz and $k_z/k_0 = 1.6286$) as for the TM and TE modes. As previously, we start from the modes of the individual waveguide and shift the dispersion curves by changing the radius to get the required mode at the target frequency and wave number. For example, we obtain the hybrid mode HE_{11} at $f = 5.6$ THz and $k_z/k_0 = 1.6286$ for the cylinder with $R = 5.732$ μm.

Let us consider the class of hybrid modes with azimuthal index 1 focusing, in particular, on the modes HE_{11}, EH_{11}, and HE_{12} (see Fig. 2). We are interested in the loss compensation for the mode pairs HE_{11}-EH_{11}, HE_{11}-HE_{12}, and EH_{11}-HE_{12} with the first mode corresponding to the cylinder with loss (Region I) and the second mode corresponding to the cylinder with gain (Region II). As shown in Fig. 8, the LC thresholds exist for all the mode pairs mentioned above and for the system parameters as follows:

(1) HE_{11}-EH_{11}—$\{R_1 = 5.732,\ R_2 = 11.44\ \mu\text{m},\ \epsilon_{r1} = \epsilon_{r2} = 12,\ \tan\delta_1 = 5\times10^{-4},\ \tan\delta_2 = -4.91\times10^{-4}\}$;

(2) HE_{11}-HE_{12}—$\{R_1 = 5.732,\ R_2 = 14.487\ \mu\text{m},\ \epsilon_{r1} = \epsilon_{r2} = 12,\ \tan\delta_1 = 5\times10^{-4},\ \tan\delta_2 = -4.33\times10^{-4}\}$;

(3) EH_{11}-HE_{12}—$\{R_1 = 11.44,\ R_2 = 14.487\ \mu\text{m},\ \epsilon_{r1} = \epsilon_{r2} = 12,\ \tan\delta_1 = 4.91\times10^{-4},\ \tan\delta_2 = -4.33\times10^{-4}\}$.

We see that the LC thresholds are reached for different distances between waveguides for every pair of modes: $d = 20.89$ μm for HE_{11}-EH_{11}; $d = 27.28$ μm for HE_{11}-HE_{12}; and $d = 16.18$ μm for EH_{11}-HE_{12}. The field profiles shown in Fig. 9 prove that there are nonzero E_z and H_z in both cylinders as expected for the hybrid modes (although contribution of the electric or magnetic field can strongly differ).

As to the hybrid modes with the azimuthal index 2, we choose the mode pairs as follows: HE_{22}-EH_{21}, HE_{22}-HE_{21}, and EH_{21}-HE_{21}. Now, unlike previous cases, the radius of the waveguide with loss should be taken larger than the radius of the cylinder with gain. For the parameters of the corresponding LC thresholds, shown in Figs. 10 and 11, we have:

(1) HE_{22}-EH_{21}—$\{R_1 = 18.7,\ R_2 = 15\ \mu\text{m},\ \epsilon_{r1} = \epsilon_{r2} = 12,\ \tan\delta_1 = 5\times10^{-4},\ \tan\delta_2 = -5.95\times10^{-4}\}$;

(2) HE_{22}-HE_{21}—$\{R_1 = 18.7,\ R_2 = 9.91\ \mu\text{m},\ \epsilon_{r1} = \epsilon_{r2} = 12,\ \tan(\delta_1) = 5\times10^{-4},\ \tan(\delta_2) = -4.65\times10^{-4}\}$;

(3) EH_{21}-HE_{21}—$\{R_1 = 15,\ R_2 = 9.91\ \mu\text{m},\ \epsilon_{r1} = \epsilon_{r2} = 12,\ \tan\delta_1 = 5\times10^{-4},\ \tan\delta_2 = -4\times10^{-4}\}$.

The distances between the waveguides corresponding to these thresholds are as follows: $d = 16.64$ μm for HE_{22}-EH_{21}; $d = 16.95$ μm for HE_{22}-HE_{21}; and $d = 20.56$ μm for EH_{21}-HE_{21}. The results in Figs. 8–11 evidence that the full loss compensation can be realized for the arbitrary hybrid modes with the same azimuthal index. The structures of the modes influence only which of the cylinders should have the larger radii—the lossy or the gainy one.

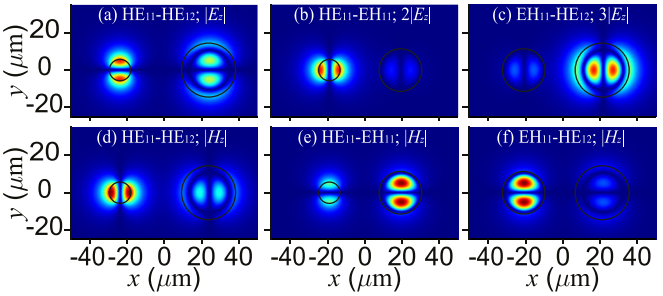

FIG. 9. (a)–(c) Electric-field $|E_z|$ corresponding to the LC thresholds of HE_{11}-HE_{12}, HE_{11}-EH_{11}, and EH_{11}-HE_{12} mode pairs; (d)–(f) The corresponding magnetic-field $|H_z|$.

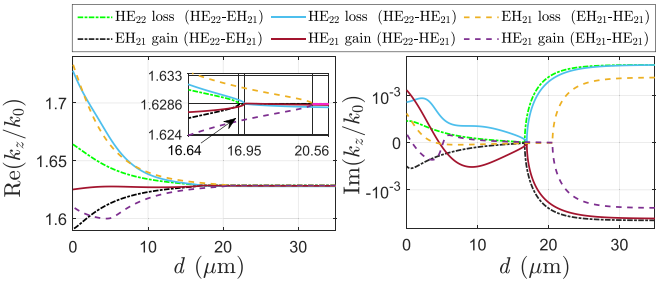

FIG. 10. Loss compensation for the hybrid modes with the azimuthal index 2.

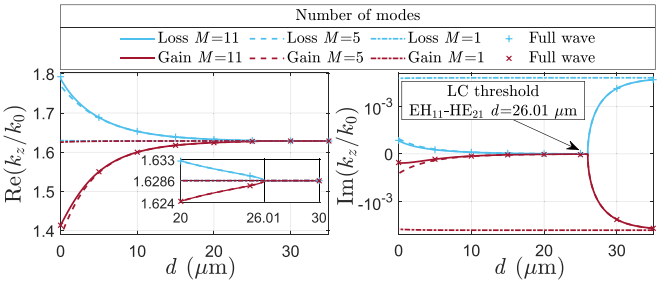

FIG. 12. Loss compensation for the hybrid modes EH_{11}-HE_{21} having different azimuthal indices.

B. Modes with different azimuthal indices

In this subsection, we study the possibility of the LC phenomenon in the coupled waveguides with loss and gain tuned to the modes with different azimuthal indices. The fundamental difference to the cases considered above is the necessity to take into account the larger number of azimuthal harmonics. For the identical azimuthal indices from the previous subsection, one can obtain the LC threshold with just one harmonic, i.e., leaving a single term in the sums of Eqs. (1)–(3). On the contrary, for the modes with different azimuthal indices, several harmonics are needed due to weak coupling between the fields (similar to the TM-TE pair).

As an example, let us consider the hybrid modes HE_{21} and EH_{11}. For their dispersion curves to cross at $f = 5.6$ THz and $k_z/k_0 = 1.6286$, the radii of the cylinders should be $R_1 = 11.44$ and $R_2 = 9.91$ μm. Figure 12 shows how the number of azimuthal harmonics in Eqs. (1)–(3) influences the possibility of the LC phenomenon for these modes. In this figure, $M = 2N + 1$ is the number of terms took into account in the field sums. We see that the LC threshold is observed for the values of $\tan\delta_1 = 6.23\times10^{-4}$ and $\tan\delta_2 = -4.65\times10^{-4}$ at the distance $d = 26.01$ μm between the waveguides only for $M \geqslant 5$, i.e., the minimal set of harmonics includes the terms with $n = \{0, \pm1, \pm2\}$. This result is confirmed by the comparison with the independent full-wave calculation using COMSOL MULTIPHYSICS® software (see the symbols in Fig. 12). The required number of harmonics becomes larger for very close cylinders (near $d = 0$) in order to save the consistency between the analytical and the numerical methods as demonstrated with the calculations for $M = 11$ in Fig. 12. Furthermore, we omit the comparison with the full-wave simulations since we are interested mainly in the region close to the LC thresholds where the consistency is perfect even for relatively small M.

Since the hybrid modes can be coupled to the symmetric TM and TE modes, we analyze the LC phenomenon for such situations as well. For the pair TM_{01}-HE_{21}, for example, the LC threshold can be reached at $d = 25.58$ μm, whereas it is $d = 28.31$ μm for TE_{01}-HE_{21} (see Fig. 13). The parameters of the system should be taken as follows:

(1) TM_{01}-HE_{21}—$\{R_1 = 10,\ R_2 = 9.91\ \mu\text{m},\ \epsilon_{r1} = \epsilon_{r2} = 12,\ \tan\delta_1 = 5\times10^{-4},\ \tan\delta_2 = -3.44\times10^{-4}\}$;

(2) TE_{01}-HE_{21}—$\{R_1 = 7.48,\ R_2 = 9.91\ \mu\text{m},\ \epsilon_{r1} = \epsilon_{r2} = 12,\ \tan\delta_1 = 5\times10^{-4},\ \tan\delta_2 = -3.32\times10^{-4}\}$;

Note that for the TM_{01}-HE_{21} pair at the LC threshold, the longitudinal electric field E_z is excited in both cylinders [Fig. 14(b)], whereas the longitudinal magnetic-field H_z exists only in the second one due to the HE_{21} mode [Fig. 14(e)]. The opposite is true for the TE_{01}-HE_{21} pair: E_z is absent in the first cylinder [Fig. 14(c)], but H_z is present in both waveguides [Fig. 14(f)].

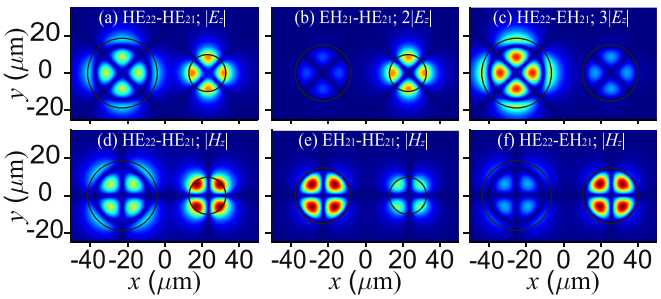

FIG. 11. (a)–(c) Electric-field $|E_z|$ corresponding to the LC thresholds of HE_{22}-HE_{21}, HE_{21}-EH_{21}, and HE_{22}-EH_{21} mode pairs; (d)–(f) The corresponding magnetic-field $|H_z|$.

V. CONCLUSION

We employ the multimode analytical approach to study the $\mathcal{PT}$ symmetry and loss-compensation phenomenon in the dielectric cylindrical waveguides with gain and loss. It is shown that for any predetermined frequency, one can realize the loss compensation by tuning the waveguides to the proper modes and to the proper radii. For the modes of either TM or TE nature, we can reach loss compensation either in the $\mathcal{PT}$-symmetric phase (when the waveguides have identical radii) or at the LC threshold (when the waveguides are dissimilar). The loss compensation is also possible in the

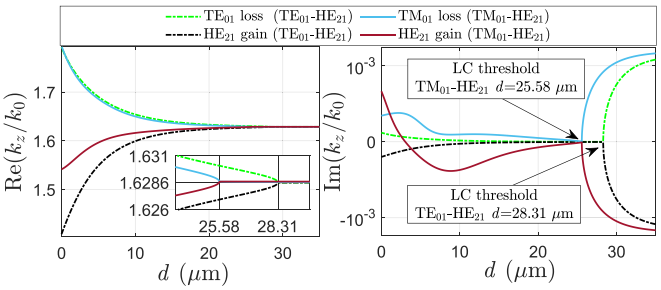

FIG. 13. Loss compensation for the circularly symmetric TM_{01}, TE_{01}, and hybrid HE_{21} modes.

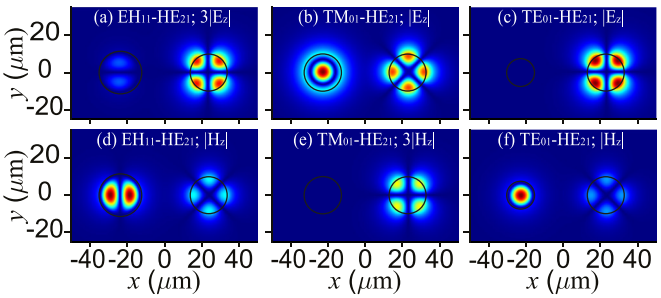

FIG. 14. (a)–(c) Electric-field $|E_z|$ corresponding to the LC thresholds of EH_{11}-HE_{21}, TM_{01}-HE_{21}, and TE_{01}-HE_{21} mode pairs; (d)–(f) the corresponding magnetic-field $|H_z|$.

situations involving the hybrid modes with identical or different azimuthal indices. By tuning the waveguides radii, we obtained the LC thresholds for a wide number of mode pairs, namely, {HE-HE, HE-EH, HE-TM, HE-TE}. The results are illustrated with the profiles of E_z and H_z components of electromagnetic field at the corresponding EPs (LC and $\mathcal{PT}$-symmetry thresholds) and corroborated by comparing with the full-wave simulations.

Our results show that the loss compensation in loss-gain systems is the general effect taking place even in asymmetric systems, such as coupled dielectric waveguides of different radii. Tuning the waveguides to the desired modes simply by changing the distance between them and their radii allows to build the lossless system starting from the arbitrary values of gain and loss. These results significantly expand the understanding of the concepts of loss compensation and $\mathcal{PT}$ symmetry and can be applied for the experimental implementation of different types of optical devices.

ACKNOWLEDGMENT

The work was supported by the National Key R&D Program of China (Project No. 2018YFE0119900) and the State Committee on Science and Technology of Belarus (Project No. F20KITG-010).

APPENDIX: DERIVATION OF TRANSVERSE FIELD COMPONENTS

The transverse field components $(E_r, H_r, E_\phi, H_\phi)$ in all regions can be readily expressed in terms of axial components Eqs. (1)–(3) from the Maxwell equations. The ϕ components of the fields in the first cylinder (Region I) can be derived as

$$E_\phi^1 = \frac{1}{k_{p,1}^2}\sum_n \left[-\frac{k_z n}{r_1}A_n^1 J_n(k_{p,1}r_1) - i\omega\mu_0 B_n^1 k_{p,1} J_n'(k_{p,1}r_1)\right]e^{in\phi_1},$$
$$H_\phi^1 = \frac{1}{k_{p,1}^2}\sum_n \left[i\omega\epsilon_1 k_{p,q} A_n^1 J_n'(k_{p,1}r_1) - \frac{k_z n}{r_1}B_n^1 J_n(k_{p,1}r_1)\right]e^{in\phi_1}, \tag{A1}$$

The ϕ components of the fields inside the second cylinder (Region II),

$$E_\phi^2 = \frac{1}{k_{p,2}^2}\sum_n \left[-\frac{k_z n}{r_2}A_n^2 J_n(k_{p,2}r_2) - i\omega\mu_0 B_n^2 k_{p,q} J_n'(k_{p,2}r_2)\right]e^{in\phi_2},$$
$$H_\phi^2 = \frac{1}{k_{p,2}^2}\sum_n \left[i\omega\epsilon_2 k_{p,2} A_n^2 J_n'(k_{p,2}r_2) - \frac{k_z n}{r_2}B_n^2 J_n(k_{p,2}r_2)\right]e^{in\phi_2}, \tag{A2}$$

For derivation of the fields in Region III, we connect the coordinates (r_1, ϕ_1) and (r_2, ϕ_2) using the Graf addition theorem,

$$B_n(r_1)e^{\pm in\phi_1} = \sum_{k=-N}^{N} B_{n+k}(h)J_k(r_2)e^{\mp ik\phi_2}e^{\pm ik\pi},$$
$$B_n(r_2)e^{\pm in\phi_2} = \sum_{k=-N}^{N} B_{n+k}(h)J_k(r_1)e^{\mp ik\phi_1}e^{\pm in\pi}, \tag{A3}$$

where B_n is the nth order cylindrical function and h is the distance between the centers of two cylinders ($h = d + R_1 + R_2$) (see Fig. 1). The ϕ components of the fields outside the cylinders in coordinates (r_1, ϕ_1) are as follows:

$$E_\phi^3(r_1,\phi_1) = \frac{1}{k_{p,3}^2}\sum_n \left\{ -\frac{k_z n}{r_1}\left[C_n^1 H_n^{(1,2)}(k_{p,3}r_1)e^{in\phi_1} + \sum_k C_n^2 H_{n+k}^{(1,2)}(k_{p,3}h)J_k(k_{p,3}r_1)e^{-ik\phi_1}e^{in\pi}\right]\right.$$
$$\left. - i\omega\mu_0 B_n^2 k_{p,3}\left[D_n^1 H_n'^{(1,2)}(k_{p,3}r_1)e^{in\phi_1} + \sum_k D_n^2 H_{n+k}^{(1,2)}(k_{p,3}h)J_k'(k_{p,3}r_1)e^{-ik\phi_1}e^{in\pi}\right]\right\},$$

$$H_{\phi}^{3}(r_1,\phi_1)=\frac{1}{k_{p,3}^2}\sum_n\left\{i\omega\epsilon_3 k_{p,3}\left[C_n^1 H_n^{\prime(1,2)}(k_{p,3}r_1)e^{in\phi_1}+\sum_k C_n^2 H_{n+k}^{(1,2)}(k_{p,3}h)J_k^{\prime}(k_{p,3}r_1)e^{-ik\phi_1}e^{in\pi}\right]\right.$$
$$\left.-\frac{k_z n}{r_1}\left[D_n^1 H_n^{(1,2)}(k_{p,3}r_1)e^{in\phi_1}+\sum_k D_n^2 H_{n+k}^{(1,2)}(k_{p,3}h)J_k(k_{p,3}r_1)e^{-ik\phi_1}e^{in\pi}\right]\right\}. \tag{A4}$$

The ϕ components of the fields in Region III in the coordinates (r_2,ϕ_2) are as follows:

$$E_{\phi}^{3}(r_2,\phi_2)=\frac{1}{k_{p,3}^2}\sum_n\left\{-\frac{k_z n}{r_2}\left[\sum_k C_n^1 H_{n+k}^{(1,2)}(k_{p,3}h)J_k(k_{p,3}r_2)e^{ik(\pi-\phi_2)}+C_n^2 H_n^{(1,2)}(k_{p,3}r_2)e^{in\phi_2}\right]\right.$$
$$\left.-i\omega\mu_0 k_{p,3}\left[\sum_k D_n^1 H_{n+k}^{(1,2)}(k_{p,3}h)J_k^{\prime}(k_{p,3}r_2)e^{ik(\pi-\phi_2)}+D_n^2 H_n^{\prime(1,2)}(k_{p,3}r_2)e^{in\phi_2}\right]\right\},$$
$$H_{\phi}^{3}(r_2,\phi_2)=\frac{1}{k_{p,3}^2}\sum_n\left\{i\omega\epsilon_3 k_{p,3}\left[\sum_k C_n^1 H_{n+k}^{(1,2)}(k_{p,3}h)J_k^{\prime}(k_{p,3}r_2)e^{ik(\pi-\phi_2)}+C_n^2 H_n^{\prime(1,2)}(k_{p,3}r_2)e^{in\phi_2}\right]\right.$$
$$\left.-\frac{k_z n}{r_2}\left[\sum_k D_n^1 H_{n+k}^{(1,2)}(k_{p,3}h)J_k(k_{p,3}r_2)e^{ik(\pi-\phi_2)}+D_n^2 H_n^{(1,2)}(k_{p,3}r_2)e^{in\phi_2}\right]\right\}, \tag{A5}$$

The explicit form of the dispersion relation is the condition of the zero determinant of the following system of equations:

$$\tilde{A}_m^1 J_m(k_{p,1}r_1)=\tilde{C}_m^1 H_m^{(1,2)}(k_{p,3}r_1)+\sum_n \tilde{C}_n^2 H_{m-n}^{(1,2)}(k_{p,3}h)J_m(k_{p,3}r_1),$$
$$B_m^1 J_m(k_{p,1}r_1)=D_m^1 H_m^{(1,2)}(k_{p,3}r_1)+\sum_n D_n^2 H_{m-n}^{(1,2)}(k_{p,3}h)J_m(k_{p,3}r_1),$$
$$\tilde{A}_m^2 J_m(k_{p,2}r_2)=\sum_n \tilde{C}_n^1 H_{m-n}^{(1,2)}(k_{p,3}h)J_m(k_{p,3}r_2)+\tilde{C}_m^2 H_m^{(1,2)}(k_{p,3}r_2),$$
$$B_m^2 J_m(k_{p,2}r_2)=\sum_n D_n^1 H_{m-n}^{(1,2)}(k_{p,3}h)J_m(k_{p,3}r_2)+D_m^2 H_m^{(1,2)}(k_{p,3}r_2),$$
$$\frac{1}{k_{p,1}^2}\left[-\frac{k_z m}{r_1}\tilde{A}_m^1 J_m(k_{p,1}r_1)-ik_0 B_m^1 k_{p,1}J_m^{\prime}(k_{p,1}r_1)\right]$$
$$=\frac{1}{k_{p,3}^2}\left\{-\frac{k_z m}{r_1}\left[\tilde{C}_m^1 H_m^{(1,2)}(k_{p,3}r_1)+\sum_n \tilde{C}_n^2 H_{m-n}^{(1,2)}(k_{p,3}h)J_m(k_{p,3}r_1)\right]\right.$$
$$\left.-ik_0 k_{p,3}\left[D_m^1 H_m^{\prime(1,2)}(k_{p,3}r_1)+\sum_n D_n^2 H_{m-n}^{(1,2)}(k_{p,3}h)J_m^{\prime}(k_{p,3}r_1)\right]\right\},$$
$$\frac{1}{k_{p,1}^2}\left[ik_0\epsilon_1 k_{p,1}\tilde{A}_m^1 J_m^{\prime}(k_{p,1}r_1)-\frac{k_z m}{r_1}B_m^1 J_m(k_{p,1}r_1)\right]$$
$$=\frac{1}{k_{p,3}^2}\left\{ik_0\epsilon_3 k_{p,3}\left[\tilde{C}_m^1 H_m^{\prime(1,2)}(k_{p,3}r_1)+\sum_n \tilde{C}_n^2 H_{m-n}^{(1,2)}(k_{p,3}h)J_m^{\prime}(k_{p,3}r_1)\right]\right.$$
$$\left.-\frac{k_z m}{r_1}\left[D_m^1 H_m^{(1,2)}(k_{p,3}r_1)+\sum_n D_n^2 H_{m-n}^{(1,2)}(k_{p,3}h)J_m(k_{p,3}r_1)\right]\right\},$$
$$\frac{1}{k_{p,2}^2}\left[-\frac{k_z m}{r_2}\tilde{A}_m^2 J_m(k_{p,2}r_2)-ik_0 B_m^2 k_{p,2}J_m^{\prime}(k_{p,2}r_2)\right]$$
$$=\frac{1}{k_{p,3}^2}\left\{-\frac{k_z m}{r_2}\left[\sum_n \tilde{C}_n^1 H_{m-n}^{(1,2)}(k_{p,3}h)J_m(k_{p,3}r_2)+\tilde{C}_m^2 H_m^{(1,2)}(k_{p,3}r_2)\right]\right.$$
$$\left.\times ik_0 k_{p,3}\left[\sum_n D_n^1 H_{m-n}^{(1,2)}(k_{p,3}h)J_m^{\prime}(k_{p,3}r_2)+D_m^2 H_m^{\prime(1,2)}(k_{p,3}r_2)\right]\right\},$$

$$\frac{1}{k_{p,2}^2}\left[ik_0\epsilon_2 k_{p,2}\tilde{A}_m^2 J_m'(k_{p,2}r_2) - \frac{k_z m}{r_2}B_m^2 J_m(k_{p,2}r_2)\right]$$
$$= \frac{1}{k_{p,3}^2}\left\{ik_0\epsilon_3 k_{p,3}\left[\sum_n \tilde{C}_n^1 H_{m-n}^{(1,2)}(k_{p,3}h)J_m'(k_{p,3}r_2) + \tilde{C}_m^2 H_m'^{(1,2)}(k_{p,3}r_2)\right]\right.$$
$$\left. - \frac{k_z m}{r_2}\left[\sum_n D_n^1 H_{m-n}^{(1,2)}(k_{p,3}h)J_m(k_{p,3}r_2) + D_m^2 H_m^{(1,2)}(k_{p,3}r_2)\right]\right\}. \quad \text{(A6)}$$

Here $\tilde{A}_n^{1,2} = \sqrt{\epsilon_0/\mu_0}A_n^{1,2}$, $\tilde{C}_n^{1,2} = \sqrt{\epsilon_0/\mu_0}C_n^{1,2}$.

[1] A. A. Zyablovsky, A. P. Vinogradov, A. A. Pukhov, A. V. Dorofeenko, and A. A. Lisyansky, PT-symmetry in optics, Phys. Usp. **57**, 1063 (2014).

[2] L. Feng, R. El-Ganainy, and L. Ge, Non-Hermitian photonics based on parity time symmetry, Nat. Photon. **11**, 752 (2017).

[3] R. El-Ganainy, K. G. Makris, M. Khajavikhan, Z. H. Musslimani, S. Rotter, and D. N. Christodoulides, Non-Hermitian physics and PT symmetry, Nat. Phys. **14**, 11 (2018).

[4] C. M. Bender and S. Boettcher, Real Spectra in Non-Hermitian Hamiltonians Having PT Symmetry, Phys. Rev. Lett. **80**, 5243 (1998).

[5] K. G. Makris, R. El-Ganainy, D. N. Christodoulides, and Z. H. Musslimani, Beam Dynamics in PT Symmetric Optical Lattices, Phys. Rev. Lett. **100**, 103904 (2008).

[6] C. E. Rüter, K. G. Makris, R. El-Ganainy, D. N. Christodoulides, M. Segev, and D. Kip, Observation of paritytime symmetry in optics, Nat. Phys. **6**, 192 (2010).

[7] J. Schindler, A. Li, M. C. Zheng, F. M. Ellis, and T. Kottos, Experimental study of active LRC circuits with $\mathcal{PT}$ symmetries, Phys. Rev. A **84**, 040101(R) (2011).

[8] X. Zhu, H. Ramezani, C. Shi, J. Zhu, and X. Zhang, $\mathcal{PT}$-Symmetric Acoustics, Phys. Rev. X **4**, 031042 (2014).

[9] M. Chitsazi, H. Li, F. M. Ellis, and T. Kottos, Experimental Realization of Floquet $\mathcal{PT}$-Symmetric Systems, Phys. Rev. Lett. **119**, 093901 (2017).

[10] O. Hess, J. B. Pendry, S. A. Maier, R. F. Oulton, J. M. Hamm, and K. L. Tsakmakidis, Active nanoplasmonic metamaterials, Nat. Mater. **11**, 573 (2012).

[11] A. Krasnok and A. Alù, Active nanophotonics, Proc. IEEE **108**, 628 (2020).

[12] D. V. Novitsky, V. R. Tuz, S. L. Prosvirnin, A. V. Lavrinenko, and A. V. Novitsky, Transmission enhancement in loss-gain multilayers by resonant suppression of reflection, Phys. Rev. B **96**, 235129 (2017).

[13] Ş. K. Özdemir, S. Rotter, F. Nori, and L. Yang, Parity-time symmetry and exceptional points in photonics, Nat. Mater. **18**, 783 (2019).

[14] M.-A. Miri and A. Alù, Exceptional points in optics and photonics, Science **363**, eaar7709 (2019).

[15] K. Ding, G. Ma, M. Xiao, Z. Q. Zhang, and C. T. Chan, Emergence, Coalescence, and Topological Properties of Multiple Exceptional Points and Their Experimental Realization, Phys. Rev. X **6**, 021007 (2016).

[16] T. Jiang and Y. Xiang, Perfectly-matched-layer method for optical modes in dielectric cavities, Phys. Rev. A **102**, 053704 (2020).

[17] X.-Y. Wang, F.-F. Wang, and X.-Y. Hu, Waveguide-induced coalescence of exceptional points, Phys. Rev. A **101**, 053820 (2020).

[18] J. Gomis-Bresco, D. Artigas, and L. Torner, Transition from Dirac points to exceptional points in anisotropic waveguides, Phys. Rev. Research **1**, 033010 (2019).

[19] A. Abdrabou and Y. Y. Lu, Exceptional points for resonant states on parallel circular dielectric cylinders, J. Opt. Soc. Am. B **36**, 1659 (2019).

[20] W. Chen, Ş. K. Özdemir, G. Zhao, J. Wiersig, and L. Yang, Exceptional points enhance sensing in an optical microcavity, Nature (London) **548**, 192 (2017).

[21] H. Hodaei, A. U. Hassan, S. Wittek, H. Garcia-Gracia, R. El-Ganainy, D. N. Christodoulides, and M. Khajavikhan, Enhanced sensitivity at higher-order exceptional points, Nature (London) **548**, 187 (2017).

[22] L. Feng, Z. J. Wong, R.-M. Ma, Y. Wang, and X. Zhang, Single-mode laser by parity-time symmetry breaking, Science **346**, 972 (2014).

[23] H. Hodaei, M.-A. Miri, M. Heinrich, D. N. Christodoulides, and M. Khajavikhan, Parity-time–symmetric microring lasers, Science **346**, 975 (2014).

[24] M. P. Hokmabadi, A. Schumer, D. N. Christodoulides, and M. Khajavikhan, Non-Hermitian ring laser gyroscopes with enhanced Sagnac sensitivity, Nature (London) **576**, 70 (2019).

[25] Y.-H. Lai, Y.-K. Lu, M.-G. Suh, Z. Yuan, and K. Vahala, Observation of the exceptional-point-enhanced Sagnac effect, Nature (London) **576**, 65 (2019).

[26] S. Longhi, $\mathcal{PT}$-symmetric laser absorber, Phys. Rev. A **82**, 031801(R) (2010).

[27] Z. J. Wong, Y.-L. Xu, J. Kim, K. O'Brien, Y. Wang, L. Feng, and X. Zhang, Lasing and anti-lasing in a single cavity, Nat. Photon. **10**, 796 (2016).

[28] D. V. Novitsky, A. Karabchevsky, A. V. Lavrinenko, A. S. Shalin, and A. V. Novitsky, $\mathcal{PT}$ symmetry breaking in multilayers with resonant loss and gain locks light propagation direction, Phys. Rev. B **98**, 125102 (2018).

[29] J. Doppler, A. A. Mailybaev, J. Böhm, U. Kuhl, A. Girschik, F. Libisch, T. J. Milburn, P. Rabl, N. Moiseyev, and S. Rotter, Dynamically encircling an exceptional point for asymmetric mode switching, Nature (London) **537**, 76 (2016).

[30] Q. Liu, S. Li, B. Wang, S. Ke, C. Qin, K. Wang, W. Liu, D. Gao, P. Berini, and P. Lu, Efficient Mode Transfer on a Compact Silicon Chip by Encircling Moving Exceptional Points, Phys. Rev. Lett. **124**, 153903 (2020).

[31] A. U. Hassan, B. Zhen, M. Soljačić, M. Khajavikhan, and D. N. Christodoulides, Dynamically Encircling Exceptional Points: Exact Evolution and Polarization State Conversion, Phys. Rev. Lett. **118**, 093002 (2017).

[32] S. Wang, B. Hou, W. Lu, Y. Chen, Z. Q. Zhang, and C. T. Chan, Arbitrary order exceptional point induced by photonic spin orbit interaction in coupled resonators, Nat. Commun. **10**, 832 (2019).

[33] Q. Zhong, J. Kou, S. K. Özdemir, and R. El-Ganainy, Hierarchical Construction of Higher-Order Exceptional Points, Phys. Rev. Lett. **125**, 203602 (2020).

[34] J. Ryu, S. Gwak, J. Kim, H.-H. Yu, J.-H. Kim, J.-W. Lee, C.-H. Yi, and C.-M. Kim, Hybridization of different types of exceptional points, Photon. Res. **7**, 1473 (2019).

[35] X.-L. Zhang and C. T. Chan, Dynamically encircling exceptional points in a three-mode waveguide system, Commun. Phys. **2**, 63 (2019).

[36] L. Jin, H. C. Wu, B.-B. Wei, and Z. Song, Hybrid exceptional point created from type-III Dirac point, Phys. Rev. B **101**, 045130 (2020).

[37] W.-P. Huang, Coupled-mode theory for optical waveguides: an overview, J. Opt. Soc. Am. A **11**, 963 (1994).

[38] D. Dai, Y. Tang, and J. E. Bowers, Mode conversion in tapered submicron silicon ridge optical waveguides, Opt. Express **20**, 13425 (2012).

[39] Z. Zhang, X. Hu, and J. Wang, On-chip optical mode exchange using tapered directional coupler, Sci. Rep. **5**, 16072 (2015).

[40] S. Kim, K. Han, C. Wang, J. A. Jaramillo-Villegas, X. Xue, C. Bao, Y. Xuan, D. E. Leaird, A. M. Weiner, and M. Qi, Dispersion engineering and frequency comb generation in thin silicon nitride concentric microresonators, Nat. Commun. **8**, 372 (2017).

[41] V. V. Klimov, I. V. Zabkov, D. V. Guzatov, and A. P. Vinogradov, Loss compensation symmetry in dimers made of gain and lossy nanoparticles, Laser Phys. Lett. **15**, 035901 (2018).

[42] A. V. Hlushchenko, V. I. Shcherbinin, D. V. Novitsky, and V. R. Tuz, Loss compensation symmetry in a multimode waveguide coupler, Laser Phys. Lett. **17**, 116202 (2020).

[43] T. P. White, B. T. Kuhlmey, R. C. McPhedran, D. Maystre, G. Renversez, C. Martijn de Sterke, and L. C. Botten, Multipole method for microstructured optical fibers. I. Formulation, J. Opt. Soc. Am. B **19**, 2322 (2002).

[44] Y. Kominis, T. Bountis, and S. Flach, The asymmetric active coupler: Stable nonlinear supermodes and directed transport, Sci. Rep. **6**, 33699 (2016).

[45] Y. Kominis, T. Bountis, and S. Flach, Stability through asymmetry: Modulationally stable nonlinear supermodes of asymmetric non-Hermitian optical couplers, Phys. Rev. A **95**, 063832 (2017).

[46] E. Snitzer, Cylindrical dielectric waveguide modes, J. Opt. Soc. Am. **51**, 491 (1961).

[47] J. W. Lamb, Miscellaneous data on materials for millimetre and submillimetre optics, Int. J. Infrared Millimeter Waves **17**, 1997 (1996).